Faraday
Discussions

Accepted Manuscript

**Faraday
Discussions**

**Royal Society of
Chemistry**

ROYAL SOCIETY
OF CHEMISTRY

ROYAL SOCIETY
OF **CHEMISTRY**

www.rsc.org/faraday_d

Faraday Discussions

PAPER

Synthesis and Strong Photooxidation Power of a Supramolecular Hybrid comprising a Polyoxometalate and Ru(II) Polypyridyl Complex with Zinc(II)

Kenji Ohashi,[a] Hiroyuki Takeda,[a] Kazuhide Koike[b] and Osamu Ishitani*[a]

A novel method for constructing supramolecular hybrids composed of polyoxometalates and photofunctional metal complexes was developed. A Ru(II) complex with phosphonate groups (**RuP**) strongly interacted with Zn(II) to afford a 2:1 trinuclear metal complex ([**(RuP)₂Zn]³⁺**). In dimethylsulfoxide, [**(RuP)₂Zn]³⁺** strongly interacted with a Keggin-type heteropolyoxometalate (**Si-WPOM**) to form a 1:1 hybrid ([**(RuP)₂Zn]-POM**). Irradiation of **[(RuP)₂Zn]-POM** in the presence of diethanolamine caused rapid accumulation of the one-electron reduced hybrid with a quantum yield of 0.99.

Introduction

Polyoxometalates (**POM**s)[1-6] are inorganic oxide clusters of early transition metals in high oxidation states (mostly d^0 and less frequently d^1 electronic configurations) with both bridging and terminal oxo ligands. **POM**s are of interest because of their applicability as acid catalysts,[7] cathodes[8] and anticancer agents[9] and their use in various electronic devices[10]. Keggin-type heteropolyoxometalates (**X-MPOM: M** = W and Mo) have one hetero atom (**X** = P, Si, As, Ge, B etc.) at their centres, and the negative charge of **X-MPOM** can be adjusted by changing the hetero atom.[11,12] These **X-MPOM**s have been used as electron acceptors in photochemical redox reactions because multiple electrons can be accumulated in each molecule, and the reduced **X-MPOM**s are relatively stable.[13,14] However, because the absorbance of **X-MPOM**s in the visible region is not much stronger than that in the ultraviolet region, joint use of another redox photosensitizer such as a Ru (II) complex is necessary for visible-light-driven photocatalytic reactions.[15] Some hybrids of photosensitizers and **X-MPOM**s linked by chemical bonds have been reported.[16] However, only a limited number of polyoxometalates can be combined with photosensitizers using this method and, if their synthesis is possible, multistep processes are required. Although ion pairs comprising **X-MPOM** with a negative charge and a cationic photosensitizer can be prepared via columbic interactions,[17,18] most readily dissociate when even a small concentration of salts is present in the solution due to the relatively low cationic charges of the photosensitizers.[19]

Herein, we report a new 2:1 hybrid of a [Ru(bpy)₃]²⁺ (bpy: bipyridyl) complex that is widely used as a photosensitizer and the Keggin-type polyoxometalate [SiW₁₂O₄₀]⁴⁻ (**Si-WPOM**). The hybrid was prepared by introducing methylphosphonate groups into the bpy ligands of the Ru complex (**RuP**), combined with the use of Zn²⁺. The hybrid has much stronger resistance to the addition of salts compared to the ion pairs formed by Ru(II) complexes (**Ru**, **RuP**) and **Si-WPOM** in the absence of Zn²⁺ and stronger photochemical oxidation power than the Ru complex alone. The structures of the compounds are shown in Fig. 1.

Results

Interaction between RuP and Zn²⁺

Fig. 2 shows ³¹P NMR spectra of **RuP** (4.4 mM) in dimethylsulfoxide (DMSO)-d₆ with and without Zn²⁺. A broad peak was observed at 15.57 ppm in the absence of Zn²⁺. Following the addition of Zn²⁺, this peak shifted to a lower magnetic field and became sharper. These changes continued

[a] Department of Chemistry, Graduate School of Science and Engineering, Tokyo Institute of Technology, Ookayama 2-12-1-NE-1, Meguro-ku, Tokyo, 152-8551, Japan. Fax: 03 5734 2240; Tel: 03 5734 2240; E-mail: iishitani@chem.titech.ac.jp

[b] National Institute of Advanced Industrial Science and Technology, Onogawa 16-1, Tsukuba, 305-8569, Japan.

† Electronic Supplementary Information (ESI) available: Detail characterization and photoproperties of products. See DOI: 10.1039/x0xx00000x
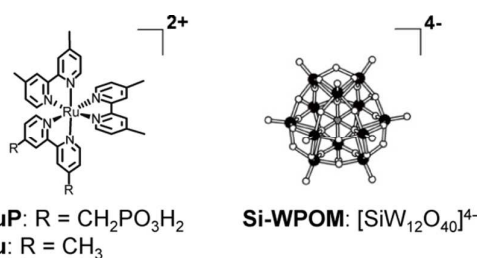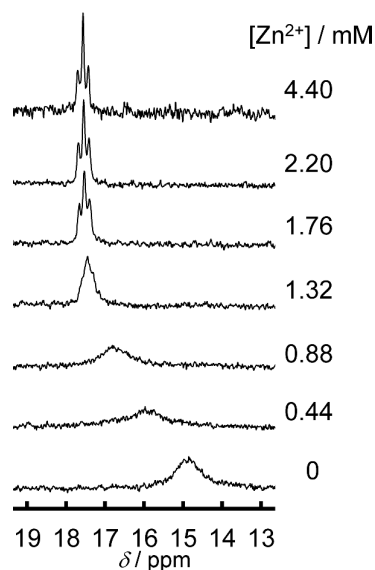
RuP: R = CH₂PO₃H₂
Ru: R = CH₃

Si-WPOM: [SiW₁₂O₄₀]⁴⁻

Fig. 1 Structures and abbreviations of the Ru(II) and polyoxometalate complexes used to prepare the new hybrids.

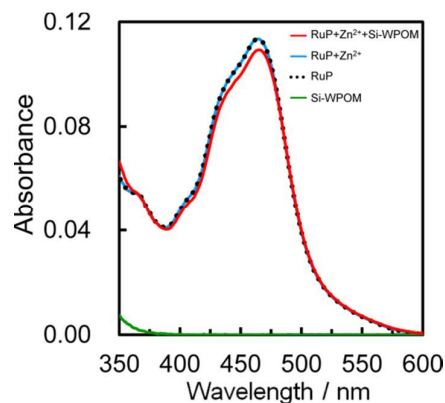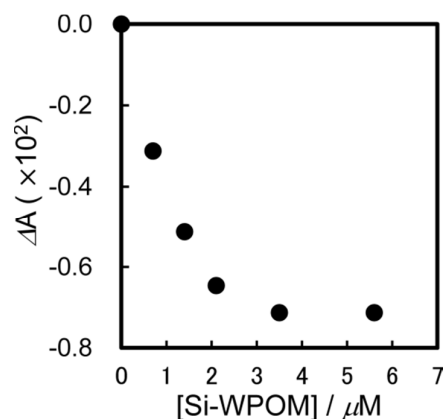**Fig. 2** ^{31}P NMR spectra of **RuP** (4.4 mM) obained in DMSO-d_6 in the absence and presence of Zn^{2+}.
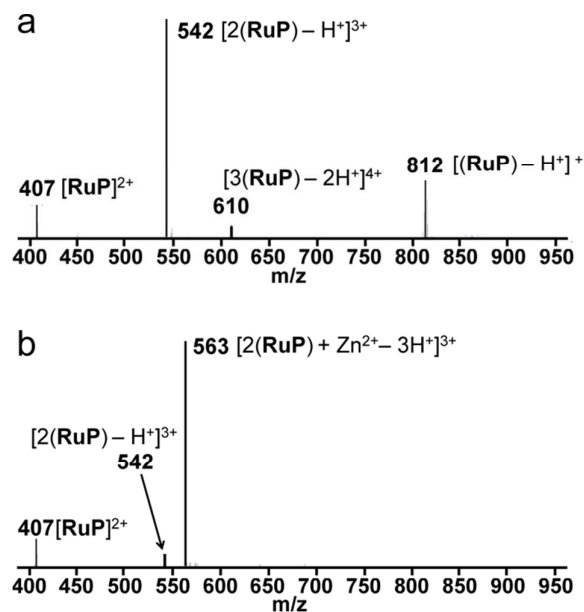
Fig. 3 ESI-MS spectra of DMSO solutions containing (a) **RuP** (4.4 mM) alone and (b) both **RuP** (4.4 mM) and Zn^{2+} (2.2 mM) (mobile phase: CH_3CN).

Fig. 4 UV-vis absorption spectra of DMSO solutions containg (black dotted line) **RuP** (7 μM) alone, (blue) both **RuP** (7 μM) and Zn^{2+} (3.5 μM), (red) **RuP** (7 μM), Zn^{2+} (3.5 μM) and **Si-WPOM** (3.5 μM) and (green) **Si-WPOM** alone.

Fig. 5 Plots of the change in absorbance at 464 nm of the mixed DMSO solution containing **RuP** (7 μM) and Zn^{2+} (3.5 μM) upon the addition of various concentrations

until the ratio between the added Zn^{2+} and **RuP** was approximately 1:2, and higher concentrations of Zn^{2+} did not further affect the peak. In the presence of 2.2 mM Zn^{2+}, the peak was observed at 17.46 ppm (J_{P-H} = 22.33 Hz). A similar sharpening of the peak for the phosphorous groups was observed upon the addition of an equal amount of trifluoromethane sulfonic acid to **RuP** (Fig. S1†). These results clearly indicate that an equilibrium existed between the deprotonated and protonated phosphorous groups in **RuP** and

that Zn^{2+} interacted with the phosphorous groups of the Ru(II) complex.

Fig. 3a presents an ESI-MS spectrum of a solution containing **RuP**. Peaks attributable to both $[\textbf{RuP}]^{2+}$ (m/z = 407) and deprotonated $[\textbf{RuP} - H^+]^+$ (m/z = 812), as well as those of the dimer and trimer (m/z = 542: $[2(\textbf{RuP}) - H^+]^{3+}$, m/z = 610: $[3(\textbf{RuP}) - 2H^+]^{3+}$) were observed. As can be seen in Fig. 3b, addition of Zn^{2+} (**RuP**:Zn^{2+} = 2:1 mol/mol) to the solution drastically changed the ESI-MS spectrum. Only one main peak was observed, at m/z = 563, which is attributable to $[2(\textbf{RuP}) + Zn^{2+} - 3H^+]^{3+}$.

**Interaction between RuP, Zn^{2+}, and Si-WPOM**

Fig. 4 shows the UV-vis absorption spectra of DMSO solutions containing **RuP** (7 μM), both **RuP** (7 μM) and Zn^{2+} (3.5 μM) and **RuP** (7 μM), Zn^{2+} (3.5 μM) and **Si-WPOM** (3.5 μM). The peak near 465 nm is attributed to metal-to-ligand charge transfer MLCT) in **RuP**. As can be seen in this figure, while the addition

Table 1 Photophysical properties of Ru(II) complexes.

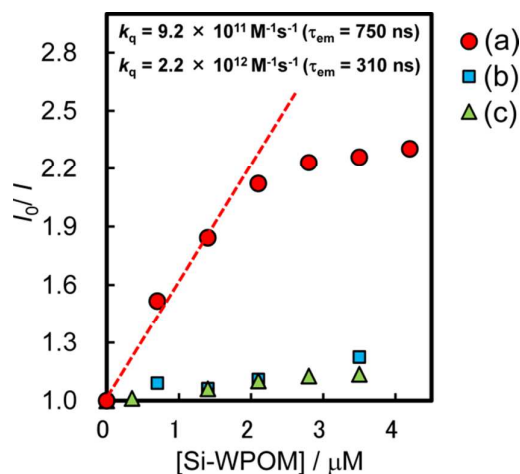| Compounds	λ_{abs} / nm (ε_{max}/ × 10^3 M^{-1} cm^{-1})	λ_{em}^{a} / nm	Φ_{em}^{a}	$\tau_{em}(A)^{a}$ / ns
RuP+Zn^{2+}+**Si-WPOM** [b]	466 (15.9)	640	0.05	670 (43%), 170 (34%), 20 (23%)
RuP+Zn^{2+} [c]	464 (16.4)	640	0.12	750 (88%), 310 (12%)
RuP	464 (16.4)	642	0.11	740 (92%), 310 (8%)
Ru	463 (15.8)	640	0.15	770 (100%)

[a]Obtained under an argon atmosphere using 510 nm excitation light. [b]Half an equivalent each of Zn^{2+} and **Si-WPOM** and 1 equivalent of **RuP** were added. [c]Half an equivalent of Zn^{2+} and 1 equivalent of **RuP** were added.
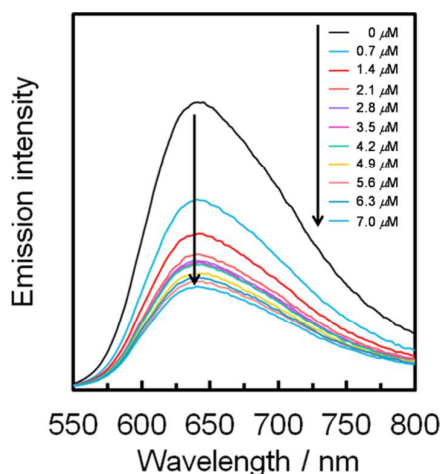
Fig. 6 Quenching of the emission from a mixed DMSO solution containing **RuP** (7 µM) and Zn^{2+} (3.5 µM) by various concentrations of **Si-WPOM** (25°C under Ar). The excitation wavelength was 510 nm. The emission intensities were normalized to the absorbance at the excitation wavelength.

Fig. 7 Stern‒Volmer plots of emission quenching from DMSO solutions of the Ru(II) complexes by **Si-WPOM**: (a ●) **RuP** (7 µM) and Zn^{2+} (3.5 µM); (b ■) **RuP** (7 µM); and (c ▲) **Ru** (7 µM) and Zn^{2+} (3.5 µM). The excitation and detection wavelengths were 510 and 630 nm, respectively.

of Zn^{2+} did not affect the absorption spectrum of **RuP**, upon addition of **Si-WPOM** to the **RuP**/Zn^{2+} solution, the **RuP** absorption maximum was slightly red-shifted and its intensity was slightly reduced (Table 1). Fig. 5 shows the change in the absorbance at λ_{abs} = 464 nm as a function of the **Si-WPOM** concentration. Notably, the intensity of the MLCT absorption band of **RuP** continued to change until the **Si-WPOM** concentration reached approximately half that of **RuP**, after which point no further changes occurred. In addition, these spectral changes were not observed in the absence of Zn^{2+}, or even in the presence of Zn^{2+} when the Ru complex did not have ligands comprising phosphorous groups (Fig. S2†).

Emission from the ^{3}MLCT excited state of **RuP** at 25°C in a DMSO solution reached a maximum at 642 nm, which was blue-shifted by 2 nm following the addition of half an equivalent of Zn^{2+}. Fig. 6 shows emission spectra for mixed solutions of **RuP** (7 µM) and Zn^{2+} (3.5 µM) in the absence and presence of various concentrations of **Si-WPOM** obtained under an Ar atmosphere following excitation at λ_{ex} = 510 nm, which was selectively absorbed by **RuP**. The emission intensity drastically decreased upon the addition of a small amount of **Si-WPOM**, although the shape of the emission spectrum did

not change. A Stern-Volmer plot of the emission quenching by **Si-WPOM** is shown in Fig. 7a. Although the emission from **RuP** in the absence of Zn^{2+} and from **Ru** in the presence of Zn^{2+} were also quenched upon addition of **Si-WPOM** (Fig. 7b and c, respectively), the quenching efficiencies were much lower compared to that for the solution containing **RuP**, Zn^{2+} and **Si-WPOM** (Fig. 7a).

Interestingly, quenching of the emission from **RuP** by **Si-WPOM** in the absence of Zn^{2+} was completely blocked upon the addition of tetrabutylammonium hexafluorophosphate (TBAPF$_6$, 10 mM) (Fig. S3†). In the presence of Zn^{2+}, however, addition of TBAPF$_6$ (10 mM) did not affect the emission quenching by **Si-WPOM** (Fig. S4†).

Fig. 8 shows the emission decay for **RuP** (7 µM, excitation at 510 nm; detection at 630 nm) in a DMSO solution containing Zn^{2+} (3.5 µM) at 25°C under an Ar atmosphere in the absence and presence of **Si-WPOM** (3.5 µM) for the same number of irradiated photons. The decay curve in the absence of **Si-WPOM** was fitted with a double exponential function, and the emission lifetimes (τ_{em}) were calculated to be 750 (the pre-exponential factor was 88%) and 310 ns (12%). On the other hand, the initial stage of the decay curve in the presence

Table 2 Redox potentials of Ru(II) complexes and **Si-WPOM**[a]

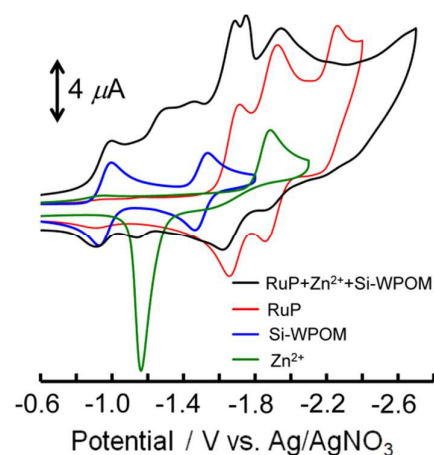| Compounds	$E_{1/2}$ / V vs. Ag/AgNO$_3$		
	$E_{1/2}^{ox}$ / V	$E_{1/2}^{red}$ / V	E_p^{red} / V
RuP+Zn^{2+}+Si-WPOM	0.88	−0.96	−1.30, −1.46, −1.68, −1.75, −1.95
RuP+Zn^{2+}	0.88	−1.62	−1.84
RuP	0.88	−1.67, −1.89, −2.21	-
Ru	0.86	−1.64, −1.81, −2.06	-
Si-WPOM	-	−0.96, −1.50	-
Zn^{2+}	-	-	−1.88

[a]Determined in DMSO containing TBAPF$_6$ (0.1 M) using a glassy carbon working electrode, a Pt counter electrode, and a Ag/AgNO$_3$ (0.01 M) reference electrode. The scan rate was 200 mV s^{-1}.
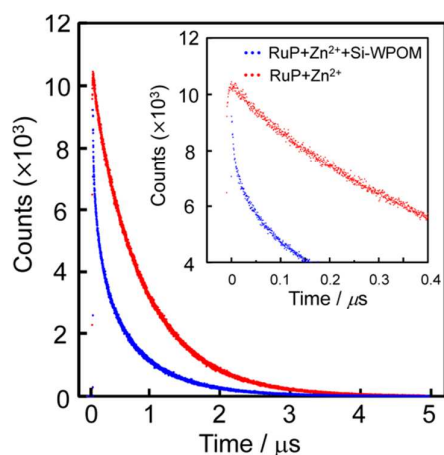
Fig. 8 Emission decays for **RuP** (7 μM, excitation at 510 nm; detection at 630 nm) in a DMSO solution containing Zn^{2+} (3.5 μM) at 25°C under an Ar atmosphere in the absence (red) and presence (blue) of **Si-WPOM** (3.5 μM) with the same number of irradiated photons. The inset shows the magnification of the initial stage.


Fig. 9 Cyclic voltammograms for DMSO solutions containing (black) **RuP** (0.5 mM), Zn^{2+} (0.025 mM) and **Si-WPOM** (0.25 mM), (red) **RuP** (0.5 mM), (blue) **Si-WPOM** (0.25 mM) and (green) Zn^{2+} (0.25 mM). All of the solutions also contained TBAPF$_6$ (0.1 M). A glassy carbon working electrode, a Pt counter electrode, and a Ag/AgNO$_3$ (0.01 M) reference electrode were used for the measurements. The scan rate was 200 mV s^{-1}.

of **Si-WPOM** (inset in Fig. 8) decreased by approximately 10% compared to that in the absence of **Si-WPOM**, and a triple exponential function was necessary to fit the decay curve (τ_{em} = 670 (43%), 170 (34%) and 20 ns (23%)). All of the photophysical data are summarized in Table 1.

Fig. 9 shows the cyclic voltammogram (CV) for a DMSO solution containing **RuP** (0.5 mM), Zn^{2+} (0.25 mM), **Si-WPOM** (0.25 mM) and TBAPF$_6$ (0.1 M) as the electrolyte. One reversible wave was observed at $E_{1/2}$ = −0.96 V vs. Ag/AgNO$_3$, which is attributed to reduction of **Si-WPOM**, i.e. [SiW$_{12}$O$_{40}$]$^{4−/5−}$.[20] At least 5 additional reduction peaks were also observed at E_p = −1.30, −1.46, −1.68, −1.75 and −1.95 V. This reduction behaviour was clearly different from a summation of the individual reduction waves for **RuP**, **Si-WPOM** and Zn^{2+}. On the other hand, a positive scan of the DMSO solution containing **RuP**, Zn^{2+}, **Si-WPOM** and TBAPF$_6$ exhibited one reversible wave at $E_{1/2}$ = +0.88 V, which is attributable to the oxidation of ruthenium (Ru$^{II/III}$).[21] Further-

more, a peak at this potential was also observed when Zn^{2+} or **Si-WPOM** was not added (Fig. S5†). On the other hand, no oxidation wave for **Si-WPOM** was observed up to 1.0 V. The electrochemical properties are summarized in Table 2.

Photochemical reduction of Si-WPOM in the hybrid system containing RuP and Zn^{2+}

A DMSO solution containing **RuP** (0.05 mM), Zn^{2+} (0.025 mM), **Si-WPOM** (0.025 mM) and diethanolamine (DEOA, 2 M) as the reductant was irradiated under an Ar atmosphere at λ_{ex} = 480 nm. In Fig. 10a, which shows the changes in the UV-vis absorption spectrum during irradiation, it can be seen that a new absorption peak appeared at $\lambda_{max} \cong$ 730 nm. This absorbance is attributable to a one-electron-reduced species (OERS) of **Si-WPOM**, because the differential spectrum of the spectra obtained before and after irradiation (Fig. 10b) was similar to that of the OERS of **Si-WPOM**
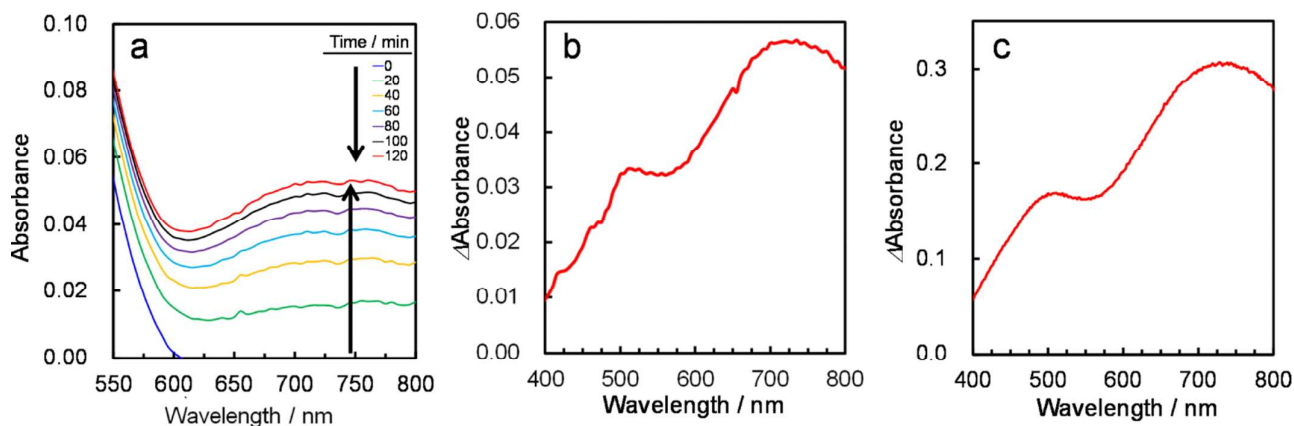
Fig. 10 (a) Changes in the absorption spectrum of an Ar-saturated DMSO solution of **RuP** (0.05 mM), Zn^{2+} (0.025 mM), **Si-WPOM** (0.025 mM) and DEOA (2 M) during irradiation (λ_{ex} = 480 nm, 20 min intervals); (b) differential spectrum obtained from the spectra for the solution before and after the irradiation for 120 min; and (c) differential absorption spectrum obtained from the spectra for **Si-WPOM** before and after reduction (1.5 mM, −1.4V vs. $Ag/AgNO_3$) using the flow electrolysis method. The analysis was conducted in a DMSO solution containing $TBAPF_6$ (0.1 M) using a glassy carbon working electrode and a Pt counter electrode. The applied potentials ranged from −0.5 and −1.6 V vs. $Ag/AgNO_3$ (0.01 M).
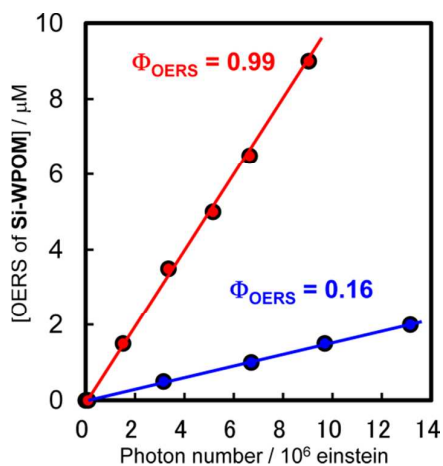

Fig. 11 Relationship between the amount of generated **Si-WPOM** OERS and the number of photons absorbed by **RuP**. DMSO solutions containing (red) 0.05 mM **RuP**, 0.025 mM Zn^{2+}, 0.025 mM **Si-WPOM** and 2 M DEOA and (blue) 0.05 mM **RuP**, 0.025 mM **Si-WPOM** and 2 M DEOA were irradiated at λ = 480 nm with a light intensity of 4.4 $\times 10^{-8}$ einstein s^{-1} under an Ar atmosphere.

produced using the flow electrolysis technique (Fig. 10c), which had a molar extinction coefficient of 2000 $M^{-1}cm^{-1}$ at λ_{abs} = 730 nm (Fig. S6†). Fig. 11 shows the relationship between the amount of **Si-WPOM** OERS produced and the number of photons absorbed by **RuP** (λ_{ex} = 480 nm, 4.4 × 10^{-8} einstein s^{-1}). This graph reveals that the formation quantum yield (Φ_{OERS}) for the **Si-WPOM** OERS was 0.99. In the absence of Zn^{2+}, conversely, Φ_{OERS} decreased to 0.16.

Discussion

Complexation of RuP and Zn^{2+}

In the ^{31}P NMR spectrum of **RuP**, the peak attributed to the phosphonate groups was broad (Fig. 2) due to the equilibrium between the protonated and deprotonated forms of the phosphorous groups. Upon addition of Zn^{2+}, this peak sharpened and shifted to a lower magnetic field. This behaviour clearly indicates that the Zn^{2+} interacted with the phosphorous groups of the **RuP**, because such interaction should lower the electron density of the phosphorous atoms. This spectral change continued until half an equivalent of Zn^{2+} was added to the solution with respect to **RuP** (Fig. 2), but further addition of Zn^{2+} did not affect the peak. The ESI-MS spectrum of a solution containing a 2:1 ratio of **RuP** and Zn^{2+} exhibited a main peak at m/z = 563, which is attributable to $[2(\mathbf{RuP}) + Zn^{2+} - 3H^+]^{3+}$. These results indicate that two molecules of **RuP** formed a complex with one molecule of Zn^{2+} in the solution to give the trivalent trinuclear complex ($[\mathbf{(RuP)_2Zn}]^{3+}$), as shown in Eq. 1.
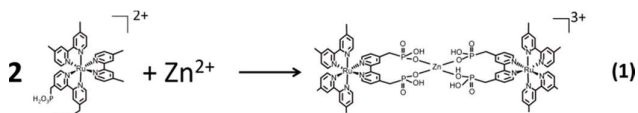
It has been reported that Zn^{2+} forms a tetrahedral coordination structure with four phosphonic acids. Therefore, it is likely that in $[\mathbf{(RuP)_2Zn}]^{3+}$, Zn^{2+} also forms a tetrahedral coordination structure with the four phosphonate groups from the two **RuP** molecules.[21] On the other hand, the ESI-MS spectrum of a solution containing Zn^{2+} and **Ru** without any phosphorous groups exhibited a main peak for $[\mathbf{Ru}]^{2+}$ (m/z = 327), but no peaks attributable to complexes between **Ru** and Zn^{2+} (Fig. S7†). Addition of Zn^{2+} did not affect the UV-vis absorption spectrum of **RuP** in DMSO solution (Fig. 4) and

caused only a 2 nm blue shift of the emission from **RuP** (Fig. S8†). Therefore, it can be concluded that complexation with Zn^{2+} did not strongly affect the electronic state of **RuP**.

Formation of a supramolecular hybrid between $[(RuP)_2Zn]^{3+}$ and Si-WPOM

The ^{1}MLCT absorption band of $[(RuP)_2Zn]^{3+}$ in the UV-vis absorption spectrum changed upon addition of **Si-WPOM** (Fig. 4). This behaviour indicates that a hybrid between $[(RuP)_2Zn]^{3+}$ and **Si-WPOM** was formed in solution. The spectral change continued until an equimolar amount of **Si-WPOM** was added to the solution of $[(RuP)_2Zn]^{3+}$; however, further addition of **Si-WPOM** had no effect on the spectrum (Fig. 5). This result indicates that reaction between one molecule of $[(RuP)_2Zn]^{3+}$ and one **Si-WPOM** proceeded in solution to afford the hybrid ($[(RuP)_2Zn]$-POM), as shown in Eq. 2.

$$[(RuP)_2Zn]^{3+} + \text{Si-WPOM} \longrightarrow [(RuP)_2Zn]^{3+} \cdots \text{Si-WPOM} \quad (2)$$
$$([(RuP)_2Zn]\text{-POM})$$
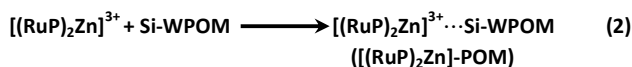
Furthermore, the addition of one equivalent of **Si-WPOM** reduced the intensity of the emission from $[(RuP)_2Zn]^{3+}$ by 56% but did not change the shape of the emission spectrum. On the other hand, the intensities of the emissions from **Ru** in the presence of Zn^{2+} and **RuP** in the absence of Zn^{2+} were only quenched by approximately 10% upon addition of the same amount of **Si-WPOM**. Stern-Volmer plots of this emission quenching, which levelled off when the concentration of added **Si-WPOM** was close to that of $[(RuP)_2Zn]^{3+}$, are shown in Fig. 7a. If dynamic quenching occurred via diffusion collisions between the excited state of $[(RuP)_2Zn]^{3+}$ and **Si-WPOM**, the emission quenching rate constants (k_q) would be 9.2×10^{11} $M^{-1}s^{-1}$ and 2.2×10^{12} $M^{-1}s^{-1}$, which were calculated from the slope at the lowest **Si-WPOM** concentration (< 1.4 μM) for the longest (τ_{em} = 750 ns) and shortest (τ_{em} = 310 ns) lifetimes, respectively, of the emission from $[(RuP)_2Zn]^{3+}$ (Fig. 7). The k_q values were obviously larger than the diffusion rate constant in DMSO (k_{diff} = 3.3×10^9 $M^{-1}s^{-1}$), which clearly indicates that the emission from $[(RuP)_2Zn]^{3+}$ was statically quenched in $[(RuP)_2Zn]$-POM.

The decays of the emissions from $[(RuP)_2Zn]$-POM and $[(RuP)_2Zn]^{3+}$ were then determined using the time-correlated single-photon counting method, and the decay curves are plotted in Fig. 8 after irradiation with the same number of photons. The initial stages of the decays (inset in Fig. 8) clearly indicate that the quenching of the excited state of $[(RuP)_2Zn]^{3+}$ by **Si-WPOM** occurred by at least one very fast process within the time resolution of the apparatus (≈ 200 ps). The decay curves could be fitted using a linear combination of several exponential functions. In the case of $[(RuP)_2Zn]$-POM, a triple exponential function was necessary to be reasonably fitted and the emission lifetimes (τ_{em}) were calculated to be 670 (44%), 170 (34%), and 20 ns (23%). On the other hand, the emission decay curve for $[(RuP)_2Zn]^{3+}$ was fitted by a double exponential function with τ_{em} = 750 (88%) and 310 ns (12%). These results suggest that there were at least 4 processes involved in the quenching of the excited state of $[(RuP)_2Zn]^{3+}$ by **Si-WPOM** in $[(RuP)_2Zn]$-POM. These processes should proceed via static quench-

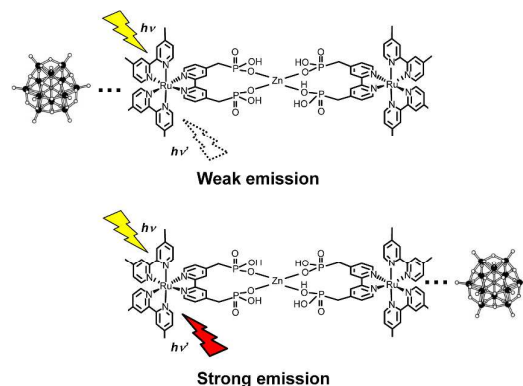**Fig. 12** Schematic representation of two possible conformers of $[(RuP)_2Zn]$-POM.

ing as described above. Therefore, there should be many conformers of $[(RuP)_2Zn]$-POM with different distances between the excited Ru(II) unit of $(RuP)_2Zn$ and the **Si-WPOM** moiety. Fig. 12 shows a schematic representation of two conformers of $[(RuP)_2Zn]$-POM; in the upper example, the **Si-WPOM** moiety is located just beside the excited Ru(II) unit, while in the lower case, the distance between the excited Ru(II) unit and the **Si-WPOM** moiety is much longer. Emission quenching in the upper case should therefore be faster than that in the lower conformer.

It is known that ion pairs comprising Ru(II) complexes and POMs readily dissociate upon the addition of salts.[23] Thus, emission quenching of **RuP** by **Si-WPOM** was not observed upon the addition of 10 mM $TBAPF_6$; i.e. the emission spectrum completely coincided with the spectrum in the absence of **Si-WPOM** (Fig. S3†). In the case of $[(RuP)_2Zn]$-POM, however, such recovery of the emission intensity was not observed following the addition of 10 mM $TBAPF_6$ (Fig. S4†). These results indicate that the ion pair formed by **RuP** and **Si-WPOM** was dissociated due to the addition of 10 mM $TBAPF_6$, while $[(RuP)_2Zn]$-POM exhibited much stronger resistance to salt addition possibly because of the higher plus charge of $[(RuP)_2Zn]^{3+}$ than that of **RuP** (2+). Furthermore, when 0.1 M $TBAPF_6$ was added to a solution of $[(RuP)_2Zn]$-POM, the emission intensity increased due to dissociation of $[(RuP)_2Zn]$-POM (Fig. S9†). However, the shape of the resultant spectrum coincided with that of $[(RuP)_2Zn]^{3+}$ (Fig. S10). Therefore, the dissociation occurred between $[(RuP)_2Zn]^{3+}$ and **Si-WPOM**, and the coordination bonds between Zn^{2+} and the phosphonate groups were maintained (Eq. 3):

$$[(RuP)_2Zn]^{3+} \cdots \text{Si-WPOM} \xrightarrow{TBAPF_6 \, (0.1 \, M)} [(RuP)_2Zn]^{3+} + \text{Si-WPOM} \quad (3)$$
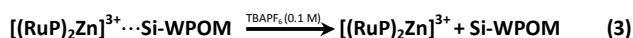
Table 3 summarizes the electrochemical properties of the excited states of $[(RuP)_2Zn]^{3+}$, **RuP**, and **Ru** (E_{red}^*, E_{ox}^*), which were obtained using Eqs. 4 and 5 and the energy gaps between the ^{3}MLCT and the ground states (E_{00}):

$$E_{red}^* = E_{red} + E_{00} \quad (4)$$

$$E_{ox}^* = E_{ox} - E_{00} \quad (5)$$

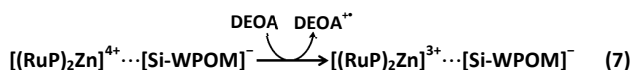**Table 3.** Electrochemical properties of the excited Ru(II) complexes[a]

Compounds	$E_{ox}*$ / V	$E_{red}*$ / V	E_{00} / eV[b]
$[(RuP)_2Zn]^{3+}$	−1.07	0.33	1.95
Ru	−1.15	0.37	2.01
RuP	−1.07	0.28	1.95

[a] Redox potentials for the ground states (E_{red}, E_{ox}) are shown in Table 1. [b]Obtained via Frank-Condon analysis[24].

For all the Ru(II) complexes, the reduction potentials of the excited states ($E_{red}*$) were more negative than the reduction potential for **Si-WPOM** ($E_{1/2}^{red}$ = −0.96 V). Consequently, electron transfer proceeded from the excited Ru(II) moieties to **Si-WPOM**, *i.e.* oxidative quenching occurred (Eq. 6).

$$[(RuP)_2Zn]^{3+}\cdots\text{Si-WPOM} \xrightarrow{h\nu} [(RuP)_2Zn]^{4+}\cdots[\text{Si-WPOM}]^- \quad (6)$$
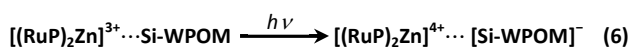
On the other hand, reductive quenching did not occur because the oxidation potentials of the excited Ru(II) moieties ($E_{ox}*$) were more negative than the oxidation potential of **Si-WPOM** (E_{ox} > 1 V). Oxidative quenching of the excited state of (**RuP**)$_2$Zn in **[(RuP)₂Zn]-POM** should result in an intramolecular charge-separated state, i.e. $[(RuP)_2Zn]^{4+}$ and $[\text{Si-WPOM}]^-$ (Eq. 6), and the one-electron oxidation states (OEOSs) of Ru complexes have stronger reduction potentials than the corresponding excited states. In fact, irradiation at λ_{ex} = 480 nm of a DMSO solution containing **[(RuP)₂Zn]-POM** and diethanolamine (DEOA) as a relatively weak electron donor efficiently produced the OERS of **Si-WPOM** (Fig. 11). In the absence of **Si-WPOM**, conversely, production of the OERS of **[(RuP)₂Zn]³⁺** was not observed (Fig. S11†). These results clearly indicate that the photochemical reduction of **[(RuP)₂Zn]-POM** proceeded via the charge-separated state, and the OEOS of the Ru complex accepted an electron from DEOA (Eq. 7).

$$[(RuP)_2Zn]^{4+}\cdots[\text{Si-WPOM}]^- \xrightarrow{\overset{\text{DEOA}\quad\text{DEOA}^{\bullet+}}{\curvearrowright}} [(RuP)_2Zn]^{3+}\cdots[\text{Si-WPOM}]^- \quad (7)$$

The quantum yield (Φ_{OERS}) for formation of the OERS of **[(RuP)₂Zn]-POM** in which the added electron was located in the **Si-WPOM** moiety, was 0.99 (Fig. 11). Furthermore, while photochemical reduction by DEOA proceeded in the absence of Zn^{2+}, *i.e.* for the **RuP/ Si-WPOM** ion pair, the Φ_{OERS} of the OERS (0.16) was 6 times less than that for **[(RuP)₂Zn]-POM**. These results demonstrate that the photooxidation power can be considerably improved via hybridization of **RuP**, Zn^{2+} and **Si-WPOM**.

Conclusion

A new, simple method for the synthesis of supramolecular hybrids composed of polyoxometalates and photofunctional metal complexes was successfully developed. Two molecules of a positively charged Ru(II) complex containing phosphonate-based ligands (**RuP**), strongly interacted with one Zn^{2+} ion to

form a trinuclear metal complex **[(RuP)₂Zn]³⁺** that strongly interacted with the polyoxometalate species (**Si-WPOM**) to form the hybrid **[(RuP)₂Zn]-POM**. Irradiation of **[(RuP)₂Zn]-POM** in the presence of a relatively weak reductant caused the accumulation of one electron in **Si-WPOM** with a good quantum yield via an intramolecular charge-separation state in **[(RuP)₂Zn]-POM**.

Experimental

General procedures

UV-vis absorption spectra were obtained using a JASCO V-565 spectrophotometer. ^1H- and ^{31}P-NMR spectra were collected in DMSO-d_6 using a JEOL ECX400IIA system (400 and 160 MHz, respectively). The residual proton of the solvent was used as the internal standard for the ^1H-NMR analyses, and the ^{31}P-NMR chemical shifts were referenced to 85% H_3PO_4. Electrospray ionization mass spectroscopy (ESI-MS) was performed using a Shimadzu LCMS-2010A system with CH_3CN as the mobile phase. Emission spectra were obtained at 25 ± 0.1°C using a JASCO FP-6500 fluorometer. The emission quantum yields and emission decays were determined using a Hamamatsu photonics C-9920-02 and a Horiba FluoroCube 1000U-S time-correlated single-photon-counting system (the excitation source was a NanoLED-510L and the instrument response was < 0.2 ns), respectively. The solutions were degassed by Ar bubbling for approximately 30 min before the emission properties were determined. Cyclic voltammograms were obtained in DMSO solutions containing each sample and N(*n*-Bu)$_4$PF$_6$ (0.1 M) as a supporting electrolyte using an ALS/CHI CHI-720 electrochemical analyzer with a glassy-carbon disk working electrode (3 mm diameter), a Ag/AgNO$_3$ (0.01 M) reference electrode, and a Pt counter electrode. The supporting electrolyte was dried in vacuo at 100°C for 1 day prior to use. The scan rate was 200 mV s^{-1}.

Photoreactions

A DMSO solution (4 mL) containing the Ru complex (0.05 mM), Zn(CF$_3$SO$_3$)$_2$ (0.025 mM), **Si-WPOM** (0.025 mM), and DEOA (2 M) was irradiated under an Ar atmosphere using an Ushio UXL-500D-O Xenon short arc lamp (500 W) combined with a 480 nm (FWHM = 10 nm) band-pass filter purchased from Asahi Spectra Co. and a CuSO$_4$ solution filter (250 g L^{-1}; pass length 5 cm). During irradiation, the temperature of the solutions was controlled at 25 ± 0.1°C using an IWAKI CTS-134A constant temperature system. For the quantum yield determinations, a Shimadzu QYM-01 quantum yield measurement system was employed and the same solution was irradiated at λ_{ex} = 480 nm under an Ar atmosphere.

Materials

DMSO was dried over 4 Å molecular sieves for several days, distilled over CaH$_2$ under reduced pressure (~ 5 mmHg), and stored under Ar prior to use. All other reagents were reagent-grade quality and used without further purification.

Synthesis

[Ru(dmb)$_2$(bmpb)](PF$_6$)$_2$ (dmb = 4,4'-dimethyl-2,2'-bipyridine, bmpb = 4,4'-bis(methyl-phosphonate)-2,2'-bipyridine),[25] [Ru(dmb)$_3$](PF$_6$)$_2$[26] and (TBA)$_4$[SiW$_{12}$O$_{40}$][20] were prepared according to the literature.

Acknowledgements

Notes and references

1   M. T. Pope, *Heteropoly and Isopoly Oxometalates*, 1983, vol. 8.
2   C. L. Hill, *Chem. Rev.*, 1998, **98**, 1–2.
3   M. T. Pope and A. Müller, Eds., *Polyoxometalate Chemistry From Topology via Self-Assembly to Applications*, Kluwer Academic Publishers, Dordrecht, 2002.
4   T. Yamase and M. T. Pope, Eds., *Polyoxometalate Chemistry for Nano-Composite Design*, Kluwer Academic Publishers, Boston, 2004.
5   J. J. Borrás-Almenar, E. Coronado, A. Müller and M. Pope, Eds., *Polyoxometalate Molecular Science*, Springer Netherlands, Dordrecht, 2003.
6   L. Cronin and A. Müller, *Chem. Soc. Rev.*, 2012, **41**, 7333–7334.
7   A. L. Kaledin, Z. Huang, Y. V Geletii, T. Lian, C. L. Hill and D. G. Musaev, *J. Phys. Chem. A*, 2010, **114**, 73–80.
8   I.-M. Mbomekallé, X. López, J. M. Poblet, F. Sécheresse, B. Keita and L. Nadjo, *Inorg. Chem.*, 2010, **49**, 7001–7006.
9   M. Sadakane and E. Steckhan, *Chem. Rev.*, 1998, **98**, 219–238.
10   T. Yamase, *Chem. Rev.*, 1998, **98**, 307–326.
11   I.-M. Mbomekallé, X. López, J. M. Poblet, F. Sécheresse, B. Keita and L. Nadjo, *Inorg. Chem.*, 2010, **49**, 7001–7006.
12   M. Sadakane and E. Steckhan, *Chem. Rev.*, 1998, **98**, 219–238.
13   A. Yokoyama, T. Kojima, K. Ohkubo, M. Shiro and S. Fukuzumi, *J. Phys. Chem. A*, 2011, **115**, 986–997.
14   K. J. Elliott, A. Harriman, L. Le Pleux, Y. Pellegrin, E. Blart, C. R. Mayer and F. Odobel, *Phys. Chem. Chem. Phys.*, 2009, **11**, 8767–8773.
15   F. Song, Y. Ding, B. Ma, C. Wang, Q. Wang, X. Du, S. Fu and J. Song, *Energy Environ. Sci.*, 2013, **6**, 1170.
16   B. Matt, J. Moussa, L. Chamoreau, C. Afonso, A. Proust, H. Amouri and G. Izzet, *Organometallics*, 2012, **31**, 35–38.
17   J. Song, Z. Luo, H. Zhu, Z. Huang, T. Lian, A. L. Kaledin, D. G. Musaev, S. Lense, K. I. Hardcastle and C. L. Hill, *Inorganica Chim. Acta*, 2010, **363**, 4381–4386.
18   J. J. Walsh, D.-L. Long, L. Cronin, A. M. Bond, R. J. Forster and T. E. Keyes, *Dalton Trans.*, 2011, **40**, 2038–2045.
19   M. K. Seery, L. Guerin, R. J. Forster, E. Gicquel, V. Hultgren, A. M. Bond, A. G. Wedd and T. E. Keyes, *J. Phys. Chem. A*, 2004, **108**, 7399–7405.
20   J. Zhang, A. M. Bond, D. R. MacFarlane, S. A. Forsyth, J. M. Pringle, A. W. A. Mariotti, A. F. Glowinski and A. G. Wedd, *Inorg. Chem.*, 2005, **44**, 5123–5132.
21   Y. Tamaki, K. Watanabe, K. Koike, H. Inoue, T. Morimoto and O. Ishitani, *Faraday Discuss.*, 2012, **155**, 115.
22   M. Wiebcke, *J. Mater. Chem.*, 2002, **12**, 421–425.
23   N. Fay, V. M. Hultgren, A. G. Wedd, T. E. Keyes, R. J. Forster, D. Leane and A. M. Bond, *Dalton Trans.*, 2006, 4218–4227.
24   K. Koike, N. Okoshi, H. Hori, K. Takeuchi, O. Ishitani, H. Tsubaki, I. P. Clark, M. W. George, F. P. a Johnson and J. J. Turner, *J. Am. Chem. Soc.*, 2002, **124**, 11448–11455.
25   Y. Ueda, H. Takeda, T. Yui, K. Koike, Y. Goto, S. Inagaki and O. Ishitani, *ChemSusChem*, 2014, **8**, 439–442.
26   B. Gholamkhass, H. Mametsuka, K. Koike, T. Tanabe, M. Furue and O. Ishitani, *Inorg. Chem.*, 2005, **44**, 2326–2336.